IEEE TRANSACTIONS ON

MAGNETICS

A PUBLICATION OF THE IEEE MAGNETICS SOCIETY

JULY 2007 VOLUME 43 NUMBER 7 IEMGAQ (ISSN 0018–9464)

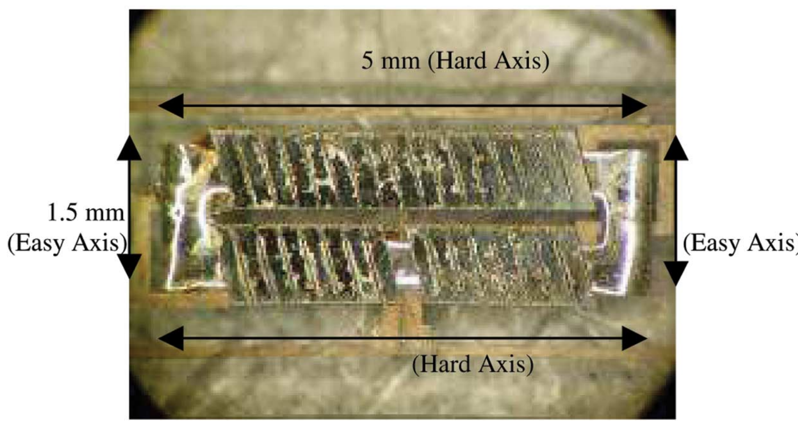

Solenoid micro-inductor, fabricated by a three-wafer process, used to characterize alloys for use at megahertz frequencies, as described in the paper "Characterization of Core Materials for Microscale Magnetic Components Operating in the Megahertz Frequency Range" by D. Flynn, A. Toon, L. Allen, R. Dhariwal, and M. P. Y. Desmulliez on page 3171. The core is assembled between the winding layers prior to flip-chip bonding. When the core is anisotropic the orientation of the easy and hard axes are indicated.

IEEE

IEEE MAGNETICS SOCIETY

The IEEE Magnetics Society is an association of IEEE members and affiliates with professional interests in the field of magnetics. All IEEE members are eligible for membership in the IEEE Magnetics Society upon payment of the annual Society membership fee of $20.00. Membership includes both electronic access to this TRANSACTIONS via IEEE Xplore and an annual TRANSACTIONS CD-ROM. Mail subscriptions to the print version are available to Society members for an additional fee of $20.00. It is possible for members of other professional societies to become Society affiliates. Information on membership can be obtained by writing to the IEEE at the address below. *Member copies of Transactions/Journals are for personal use only*.

IEEE TRANSACTIONS ON MAGNETICS (ISSN 0018-9464) is published monthly by The Institute of Electrical and Electronics Engineers, Inc. Responsibility for the contents rests upon the authors and not upon the IEEE, the Society, or its members. **IEEE Corporate Office:** 3 Park Avenue, 17th Floor, New York, NY 10016-5997. **IEEE Operations Center:** 445 Hoes Lane, P. O. Box 1331, Piscataway, NJ 08855-1331. **N.J. Telephone:** +1 732 981 0060. **Price/Publication Information:** Individual copies: IEEE Members $20.00 (first copy only), nonmembers $77.00 per copy. (Note: Postage and handling charge not included.) Member and nonmember subscription prices available upon request. Available in microfiche and microfilm. **Copyright and Reprint Permissions:** Abstracting is permitted with credit to the source. Libraries are permitted to photocopy for private use of patrons, 1) those post-1977 articles that carry a code at the bottom of the first page, provided the per-copy fee indicated at the bottom of the first page in the code is paid through the Copyright Clearance Center, 222 Rosewood Drive, Danvers, MA 01923. 2) For all other copying, reprint, or republication permission, write to: Copyrights and Permissions Department, IEEE Publications Administration, 445 Hoes Lane, P.O. Box 1331, Piscataway, NJ 08855-1331. Copyright © 2007 by The Institute of Electrical and Electronics Engineers, Inc. All rights reserved. Periodicals Postage Paid at New York, NY and at additional mailing offices. **Postmaster:** Send address changes to IEEE TRANSACTIONS ON MAGNETICS, IEEE, 445 Hoes Lane, P. O. Box 1331, Piscataway, NJ 08855-1331. GST Registration No. 125634188. Printed in U.S.A.

Digital Object Identifier 10.1109/TMAG.2007.902229

IEEE TRANSACTIONS ON

MAGNETICS

A PUBLICATION OF THE IEEE MAGNETICS SOCIETY

JULY 2007 VOLUME 43 NUMBER 7 IEMGAQ (ISSN 0018-9464)

PAPERS

(Contents Continued on Page 3142)

(Contents Continued from Page 3141)

Finite-Element Time-Step Simulation of the Switched Reluctance Machine Drive Under Single Pulse Mode Operation

M. J. Kamper, S. W. Rasmeni, and R.-J. Wang

Department of Electrical and Electronic Engineering, University of Stellenbosch, Matieland 7602, South Africa

This paper proposes two distinct numerical simulation methods using finite-element time-step analysis for predicting the current waveform of a switched reluctance machine drive and explains them in detail. It evaluates and compares the methods in terms of waveform results and simulation time, with the focus on only single pulse mode operation. The paper also reviews important factors that affect the simulated current waveforms. It presents and compares measured and simulated multi-phase current waveforms of a 49 kW switched reluctance machine drive under single pulse mode operation.

***Index Terms*—Finite element method, simulation, single pulse mode, switched reluctance machine.**

I. Introduction

The switched reluctance machine (SRM) has been a popular option for high-speed operation due to its simple and robust rotor construction. Under high-speed operation, the SRM drive operates in the so-called single pulse mode. In this mode, the drive's power electronic converter (Fig. 1) is used to apply positive dc bus voltage to the phase winding of the machine by switching Q_1 and Q_2 on for the whole switched-on or excitation time of the phase winding. During switching-off, both Q_1 and Q_2 are switched off and the phase winding voltage becomes momentarily negative to $-V_{\rm dc}$ as the phase winding demagnetizes through the freewheel diodes D_1 and D_2.

As a result of the above single pulse mode switching, the phase winding current and the generated torque of the machines are no longer under control and are determined purely by the bus voltage, flux linkage, rotor position, and speed of the machine. It is thus important to predict accurately the phase current and torque of the SRM when investigating the performance and hence the design of the machine under single pulse mode operation.

The conventional method of solving for the current and torque of the SRM is first to obtain a complete set of flux linkage data of the machine through measurements or finite-element (FE) analysis. This data is then used to solve for the phase winding current by means of interpolating polynomials (curve fitting), lookup tables, and numerical methods, and to calculate the torque [1]–[5]. The advantage of this method is that the current and torque response can be simulated quickly for all operating conditions of the machine once the curve fitting and other derivations have been done. The disadvantage of this method is that accurate simulation and torque calculation become more difficult to achieve when two or more phases are active and there is mutual magnetic coupling between the phases. Moreover, for accurate simulation taking mutual coupling into account by this method, the number of FE solutions required obtaining a complete set of flux linkage data for all possible combinations of phase currents and rotor positions become excessive.

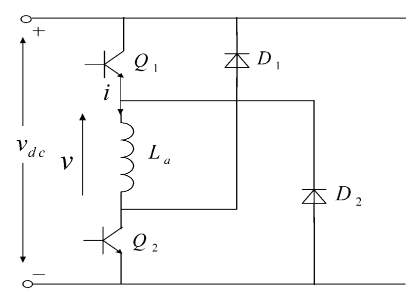

Fig. 1. Per phase power circuit of SRM drive.

The other method, called the coupled field-circuit method or FE time-stepping method [6]–[13], uses the FE solution actively in solving the circuit and mechanical state equations. Thus, this method does not need a set of precalculated flux linkage data. In [6] an inductance matrix as a function of position is determined and used in the partial differential state equation to solve for the currents. Mutual coupling between the phase windings, however, is not properly considered and the inductance matrix is only determined at a certain load-level. In [8] an iterative process, which includes mutual coupling, is used to solve the terminal voltage state equation. The numerical convergence process, however, is not explained and might be computationally expensive. References [9] and [10] give simulation results obtained from using commercial packages and the actual numerical solution methods are not described. In [11] the circuit and magnetic field variables, in a step forward, are solved simultaneously with the FE method. The rotor speed in this method is constant and the mechanical system cannot be readily accounted for. Furthermore, [11] does not give any detail regarding the accuracy and computation time of their method in comparison with others. There are also clear errors in the simulated current and torque waveform results under single pulse mode operation.

In this paper, we present two methods that use separate magnetostatic FE field solutions in solving the circuit and mechanical equations of the system. The two methods are improvements of the methods of [6], [8] and take mutual coupling and the state of the mechanical system into account. Important computational aspects that affect the accuracy and computation time of the FE simulation are shown for the first time.

Digital Object Identifier 10.1109/TMAG.2007.892792

Color versions of one or more of the figures in this paper are available online at http://ieeexplore.ieee.org.

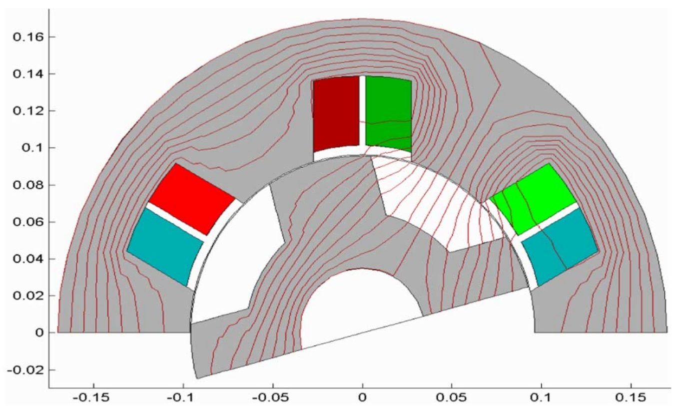

Fig. 2. Cross section and finite element field solution of three-phase tapered stator pole SRM at the unaligned ($\theta = 0^\circ$) position.

TABLE I
MAIN DIMENSIONS AND RATED VALUES OF SRM

Stator stack outer diameter	340 mm
Stack axial length	175 mm
Rotor diameter	191.4 mm
Air gap length	0.62 mm
Phase resistance	0.13 Ω
Rated amplitude of phase current	108 A
Rated torque (average)	312 Nm
Rated power at 1500 r/min	49 kW

II. FINITE-ELEMENT MODEL OF SRM

The 2-D FE software used in the current waveform simulation scheme is not of the commercial variety. It makes use of triangular elements of the first order. Only half of the machine is meshed. To enable free rotor movement, the air gap region is not meshed. Instead, the air-gap macro-element proposed by [14] is used comprising nodes on both sides of the air gap. To minimize the calculation time the technique described in [15] has been implemented with negative boundary conditions imposed. The *inputs* to the FE program are the phase current(s) i and rotor position θ of the machine. The FE program then uses a nonlinear solution procedure to solve for the magnetic vector potential at the different nodes. From the known nodal vector potentials the flux linkage(s) λ and torque T of the machine are calculated. These two parameters (λ and T) are the *outputs* of the FE program, which are used by the simulation program to predict the phase current(s) of the machine. Shown in Fig. 2 is an example of a field plot resulting from the FE solution for a conventional SRM [16]. The main dimensions and rated values of the SRM are given in Table I.

III. SIMULATION METHODS

Two different FE time-step simulation methods are proposed and explained in this section. The methods are called the *vector direction* method and the *partial differential* method.

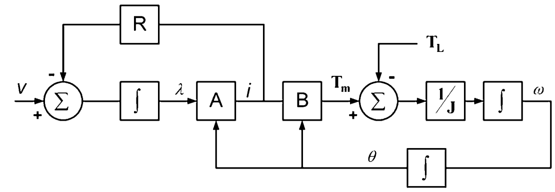

Fig. 3. Simulation block diagram of SRM-system with one phase active.

A. Vector Direction Method

Ignoring friction, the following first-order differential equations describe the system

$$v_j = Ri_j + \frac{d\lambda_j}{dt} \tag{1}$$

$$T - T_L = J\frac{d\omega}{dt} \tag{2}$$

$$\frac{d\theta}{dt} = \omega \tag{3}$$

where v_j, i_j, and λ_j are the voltage, current, and flux linkage, respectively, of the jth phase of the SRM; T, T_L, J, ω, and θ are respectively the machine torque, load torque, inertia, speed, and rotor position of the machine-system. If only one phase of the SRM is active, then these equations can be represented by the simulation block diagram of Fig. 3. The inputs of the system are the voltage ($v = V_{\rm dc}$ during switching on and $v = -V_{\rm dc}$ during switching off under single pulse mode operation) and the load torque. The outputs of the system are current, torque, and speed. For the integrators of Fig. 3, the Euler integration is used in the time-step simulation. Hence, the flux linkage and speed derivatives are determined by approximation as

$$\frac{d\lambda_j}{dt} \approx \frac{\lambda_j^{n+1} - \lambda_j^n}{\Delta t} \tag{4}$$

$$\frac{d\omega}{dt} \approx \frac{\omega_{n+1} - \omega_n}{\Delta t} \tag{5}$$

where n is the time-step number; $\lambda_{\rm n+1}$ and ω_{n+1} are the new flux linkage and speed respectively at time-step $n+1$. Substituting (4) and (5) into (1) and (2) results in

$$\lambda_j^{n+1} = \left(v_j^n - Ri_j^n\right)\Delta t + \lambda_j^n \tag{6}$$

$$\omega_{n+1} = \frac{1}{J}\left(T_n - T_L^n\right)\Delta t + \omega_n. \tag{7}$$

The new rotor position is determined from the relation

$$\theta_{n+1} = \omega_n \Delta t + \theta_n. \tag{8}$$

All system variables are known at time-step n so that the new values of flux linkage, speed, and rotor position can immediately be determined according to (6)–(8); note that the use of (6) is one aspect that fundamentally distinguishes the vector direction method from the method in [8]. What is unknown are the new currents i_j^{n+1} and torque T_{n+1}. The very heart of the vector direction simulation method is functional block A of Fig. 3 where

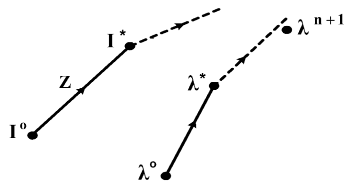

Fig. 4. Moving the flux linkage position vector $\boldsymbol{\lambda}$ by moving the current position vector $\mathbf{I}$ through vector direction $\mathbf{Z}$.

flux linkage is converted to current. In functional block B current is converted to torque. The functional blocks are described in the following sections.

Current Calculation (Functional Block A): The generated phase flux linkages in the machine is a nonlinear function of the phase currents, that is

$$\boldsymbol{\lambda} = F(\mathbf{I}) \tag{9}$$

where λ and $\mathbf{I}$ are column vectors

$$\boldsymbol{\lambda} = \begin{bmatrix} \lambda_1 \\ \lambda_2 \\ \vdots \\ \lambda_m \end{bmatrix}; \quad \mathbf{I} = \begin{bmatrix} i_1 \\ i_2 \\ \vdots \\ i_m \end{bmatrix} \tag{10}$$

and m the number of phases of the machine. What is known is the new flux linkage vector $\boldsymbol{\lambda}^{\mathbf{n+1}}$ and the old current vector $\mathbf{I^n}$ (at time-step n); what is unknown is the new current vector $\mathbf{I^{n+1}}$ that has to generate $\boldsymbol{\lambda}^{\mathbf{n+1}}$ according to (9). To solve for the new currents, it is important to first rotate the rotor in the FE analysis to its new position θ_{n+1} calculated according to (8). At this new rotor position and using an initial current position vector $\mathbf{I^o} = \mathbf{I^n}$ in the FE program, a flux linkage position vector $\boldsymbol{\lambda}^{\mathbf{o}}$ is calculated through FE analysis. Next, the current position vector in the current space is moved in a vector direction $\mathbf{Z}$ from its initial position vector $\mathbf{I^n}$ to a new position vector $\mathbf{I}^*$, i.e.,

$$\mathbf{I}^* = \mathbf{I^o} + \mathbf{Z}. \tag{11}$$

This will move the flux linkage position vector in the flux linkage space from the initial position vector $\boldsymbol{\lambda}^{\mathbf{o}}$ to a new position vector $\boldsymbol{\lambda}^*$ that is at or close to the target flux linkage position vector $\boldsymbol{\lambda}^{\mathbf{n+1}}$ (see Fig. 4). If

$$\left|\lambda_j^{n+1} - \lambda_j^*\right| \leq \xi \left|\lambda_j^{n+1}\right| \tag{12}$$

for each jth phase, where ξ is a fractional tolerance in the flux linkage value, then $\mathbf{I^{n+1}} = \mathbf{I}^*$. If not, a next iteration with a new current vector direction $\mathbf{Z}$ and $\mathbf{I^o} = \mathbf{I}^*$ is executed.

To determine the current direction vector $\mathbf{Z}$ of (11) in a mutually coupled magnetic circuit, the following differential equation at the position vector $\mathbf{I^o}$ can be used:

$$\mathrm{d}\boldsymbol{\lambda}^{\mathbf{o}} = \mathbf{L_o}\mathrm{d}\mathbf{I^o} \tag{13}$$

where $\mathrm{d}\boldsymbol{\lambda}^{\mathbf{o}}$ and $\mathrm{d}\mathbf{I^o}$ are differential flux linkage and current position vectors and $\mathbf{L_o}$ is an inductance matrix given by

$$\mathbf{L_o} = \begin{bmatrix} \frac{\partial\lambda_1^o}{\partial i_1^o} & \frac{\partial\lambda_1^o}{\partial i_2^o} & \cdots & \frac{\partial\lambda_1^o}{\partial i_m^o} \\ \frac{\partial\lambda_2^o}{\partial i_1^o} & \frac{\partial\lambda_2^o}{\partial i_2^o} & \cdots & \frac{\partial\lambda_2^o}{\partial i_m^o} \\ \vdots & & & \vdots \\ \frac{\partial\lambda_m^o}{\partial i_1^o} & \frac{\partial\lambda_m^o}{\partial i_2^o} & \cdots & \frac{\partial\lambda_m^o}{\partial i_{1m}^o} \end{bmatrix}. \tag{14}$$

From (13), the current direction vector is determined as

$$\mathbf{Z} = \mathrm{d}\mathbf{I^o} = \mathbf{L_o^{-1}}[\boldsymbol{\lambda}^{\mathbf{n+1}} - \boldsymbol{\lambda}^{\mathbf{o}}]. \tag{15}$$

The elements of $\mathbf{L_o}$ can be determined by using the forward difference approximation

$$\frac{\partial\lambda_j^o}{\partial i_i^o} = \frac{\lambda_j^o\left(i_i^o + \Delta i\right) - \lambda_j^o\left(i_i^o\right)}{\Delta i} \tag{16}$$

and calculating the flux linkages of (16) through FE method; note that m FE field solutions are required to determine $\mathbf{L_o}$. In (12) the fractional tolerance ξ is set at $\xi = 0.01$, i.e., if all the flux linkages are within 1% of the target flux linkages, the currents are accepted as a solution. Our experience is that a second iteration seldom occurs to solve for the currents if the time-step is small.

Torque Calculation (Functional Block B): The inputs to functional block B of Fig. 3 are the current, i (determined by functional block A), and the rotor position, θ, of the machine. With these inputs known, functional block B calls the FE program to accurately calculate the torque T_m of the machine.

To solve for the current (functional block A in Fig. 3) and the torque (functional block B) will require $k(m+1)$ FE solutions, where k is the number of iterations needed to satisfy (12) [typically $k = 1, 2$]. Thus, with say two phases active ($m = 2$), a minimum of three FE field solutions per time-step will be required to solve the block diagram of Fig. 3.

It is important to note that the solved reluctivities of the nonlinear FE field solution of the previous iteration or time step are used in the field solution of the next iteration and time step. This saves a lot of simulation time as the previous reluctivity values are already close to the next (new) reluctivity values.

B. Partial Differential Simulation Method

In the partial differential simulation method the new current vector $\mathbf{I^{n+1}}$ is predicted using an expanded form of (1). The flux linkage is a function of i and θ, and these are in turn functions of time so that (1) can be expanded using the principle of super position as

$$v_j = Ri_j + \frac{\partial\lambda_j}{\partial i_1}\frac{di_1}{dt} + \cdots + \frac{\partial\lambda_j}{\partial i_j}\frac{di_j}{dt} + \cdots + \frac{\partial\lambda_j}{\partial i_m}\frac{di_m}{dt} + \frac{\partial\lambda_j}{\partial\theta}\frac{d\theta}{dt}. \tag{17}$$

For m phases, (17) can be expressed in matrix format at time step n as

$$\mathbf{V^n} = \mathbf{RI^n} + \mathbf{L_n}\frac{d\mathbf{I^n}}{dt} + \mathbf{K_n}\omega_n \tag{18}$$

where $\mathbf{R}$, a resistance scalar matrix, and $\mathbf{K_n}$, a speed-voltage-constant column matrix, are given by

$$\mathbf{R} = \begin{bmatrix} R & 0 & \cdots & \cdots & 0 \\ 0 & R & 0 & \cdots & 0 \\ \vdots & 0 & \ddots & & \vdots \\ \vdots & \vdots & & R & 0 \\ 0 & 0 & \cdots & 0 & R \end{bmatrix}; \quad \mathbf{K_n} = \begin{bmatrix} \frac{\partial \lambda_1^n}{\partial \theta} \\ \frac{\partial \lambda_2^n}{\partial \theta} \\ \vdots \\ \frac{\partial \lambda_m^n}{\partial \theta} \end{bmatrix} \tag{19}$$

and $\mathbf{L_n}$ is the inductance matrix given by (14). Using Euler's method with Δt the step size, the current vector direction is determined from (18) as

$$\mathbf{dI^n} = \mathbf{L_n^{-1}}[\mathbf{V^n} - \mathbf{RI^n} - \mathbf{K_n}\omega^n]\Delta t \tag{20}$$

so that the new position vector current, $\mathbf{I^{n+1^*}}$, is predicted by

$$\mathbf{I^n + 1^*} = \mathbf{I^n} + \mathbf{dI^n}. \tag{21}$$

For a better current prediction, however, the *improved Euler's method* (also called *Heun's method* or *second-order Runge-Kutta method*) is used. For this, $\mathbf{dI^{n+1^*}}$ is determined in the same way as in (20), but at a new speed, ω^{n+1}, and new rotor position, θ^{n+1}, according to (7) and (8), so that the new current vector, $\mathbf{I^{n+1}}$, is determined by

$$\mathbf{I^{n+1}} = \mathbf{I^n} + \frac{\mathbf{dI^n} + \mathbf{dI^{n+1^*}}}{2}. \tag{22}$$

With the knowledge of the new currents and new rotor position, the new motor torque, T^{n+1}, is determined by means of the FE method. The elements of $\mathbf{L_n}$ are determined in the same way as in (16). Also the elements of $\mathbf{K_n}$ of (19) are determined by the forward difference approximation as

$$\frac{\partial \lambda_j^n}{\partial \theta} \approx \frac{\lambda_j^n(\theta^n + \Delta\theta) - \lambda_j^n(\theta^n)}{\Delta\theta}. \tag{23}$$

Note that [6] also makes use of the format of (17), but the determination of the inductance matrix and the use of (18) are completely different and more correct in this paper as saturation and mutual coupling between the phases are taken into account.

Considering the number of FE solutions per time-step required for the partial differential simulation method, $m+1$ FE solutions are required to calculate $\mathbf{L_n}$ and $\mathbf{K_n}$ and hence $\mathbf{dI_n}$ and $\mathbf{I^{n+1^*}}$. For the improved Euler method one FE solution is first required to determine $\boldsymbol{\lambda}^{\mathbf{n+1^*}}$, followed by $m+1$ solutions to calculate $\mathbf{dI^{n+1^*}}$ and $\mathbf{I^{n+1}}$ of (22) [the idea of also using $\mathbf{L_n}$ and $\mathbf{K_n}$ to determine $\mathbf{dI^{n+1^*}}$ to save $m+1$ solutions cannot work as matrix values rapidly vary with rotor position]. One FE solution is required to calculate the new motor torque and new flux linkage vector $\boldsymbol{\lambda}^{\mathbf{n+1}}$. Hence, a total of $2m+4$ FE solutions are required per time step for this method. This number of solutions seems to be considerably higher than in the case of the vector direction method; it depends, however, very much on the step size and accuracy of the simulation.

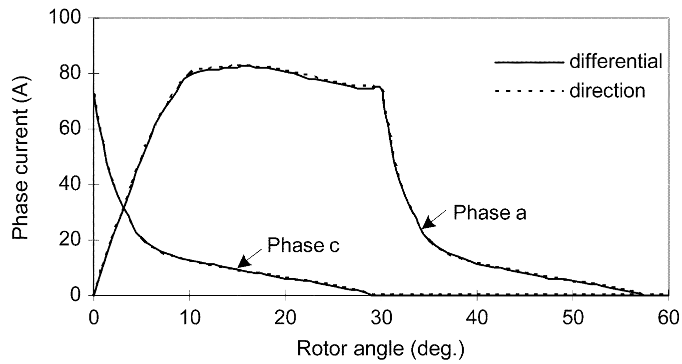

Fig. 5. Simulated current waveforms under SPMO with one-degree step size.

IV. Simulation Results

To compare the two simulation methods, the single pulse mode operation (SPMO) of the 49 kW SRM of Fig. 2 is simulated by taking the speed, and hence the rotor position step size, as constant. The speed is set at 1500 r/min and a dc bus voltage of 500 V is used.

The FE time-step simulation results of the current waveforms under SPMO are shown in Figs. 5–7. In Fig. 5 it is shown that at zero degree rotor position, as shown in Fig. 2, phase c is switched off and phase a is switched on. At 30° rotor position phase a is switched off and phase b (not shown) is switched on. The multiphase operation is clear from Fig. 5. The figure shows that there is no difference in the simulation results of the two methods for a one degree step size, but Fig. 6 shows that with a five-degree step size the partial differential method has a larger deviation. Fig. 7 confirms that the improved Euler method must be used in the partial differential simulation method.

Three aspects that affect the current waveform simulation under SPMO are investigated in the following sections. In this investigation, only the vector direction method is used.

A. Effect of Mesh

For the FE modeling of the SRM, the mesh profile could have significant influence on the accuracy of the field solution. To investigate the effect of the mesh on the simulation result, the FE models with different mesh densities as shown in Figs. 8 and 9 are used in the FE time step current waveform simulation. The current waveform simulation results are compared in Fig. 10. It is clear that the mesh profile has a substantial effect on the simulation result, especially in the regions where the stator and rotor poles overlap. Hence, the mesh profile must be considered with care, specifically in the stator and rotor pole tip areas (see

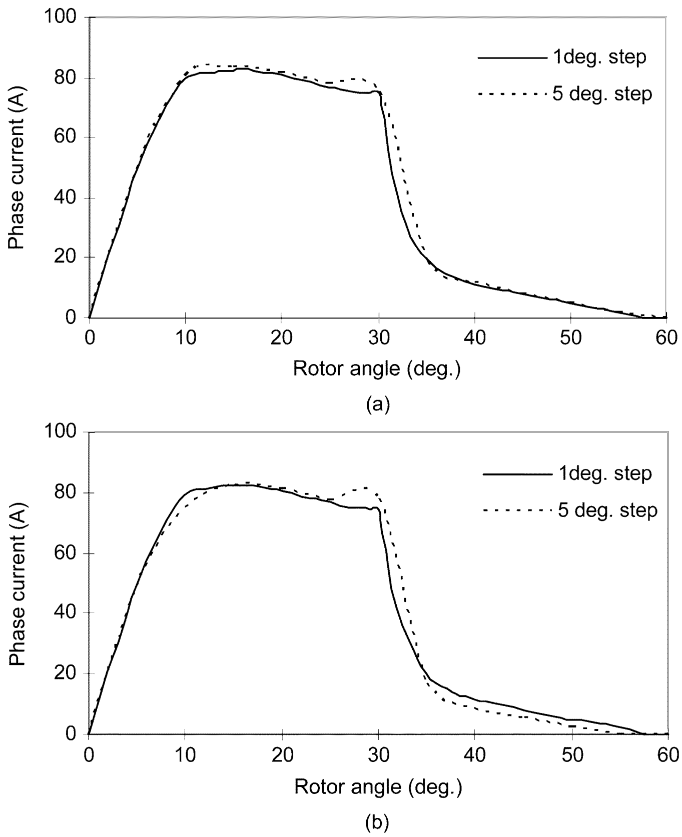

Fig. 6. Effect of five-degree step size on the simulated current waveforms under SPMO. (a) Vector direction method. (b) Partial differential method.

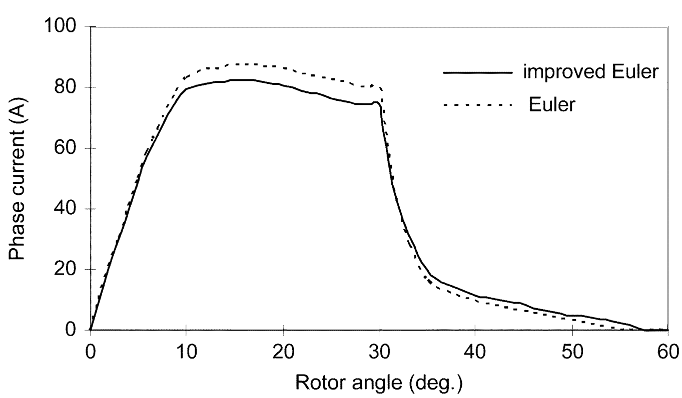

Fig. 7. Effect of Euler and improved Euler method on the simulated current waveform (partial differential method).

Fig. 9) where the transition between high permeability (iron) and low permeability (air) takes place.

B. *Effect of BH-Data*

The effect of the BH-data used in the FE solution on the simulation results is also investigated. Two BH-curves, resulting from BH-data of two different steel materials, are shown in Fig. 11. The effect of using these BH-curves in the FE analysis on the current waveform simulation results is clear from Fig. 12. The effect is shown only when the rotor and the active stator poles approach alignment that is in the region where magnetic saturation occurs. This may be explained as follows:

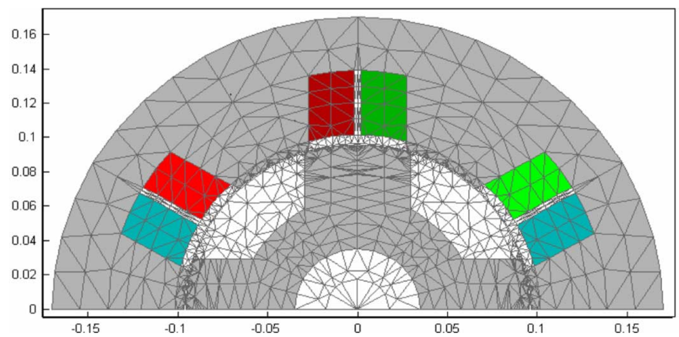

Fig. 8. FE model of SRM with less dense mesh structure.

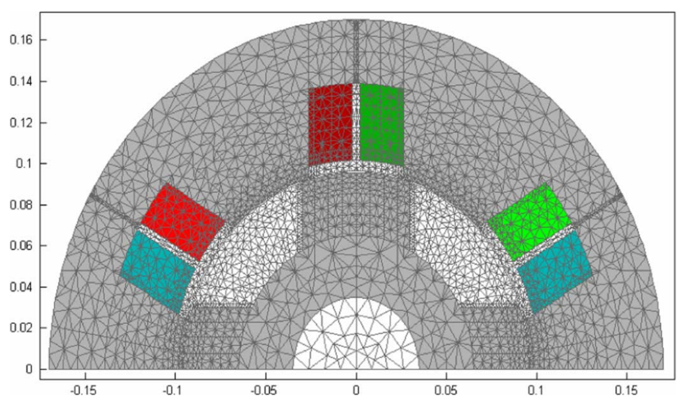

Fig. 9. FE model of SRM with high dense mesh structure.

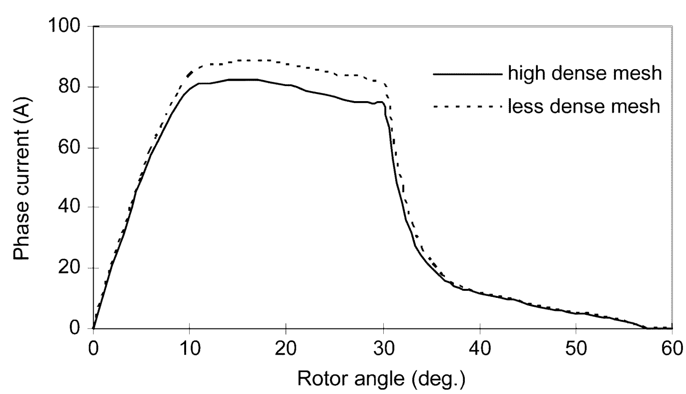

Fig. 10. Effect of mesh on the simulated current waveform.

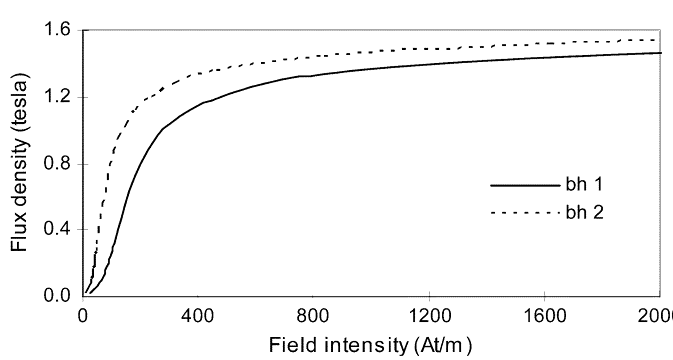

Fig. 11. BH-curves used in the FE analysis.

the flux density in the steel material with a higher permeability is generally higher resulting in a higher flux and flux linkage in

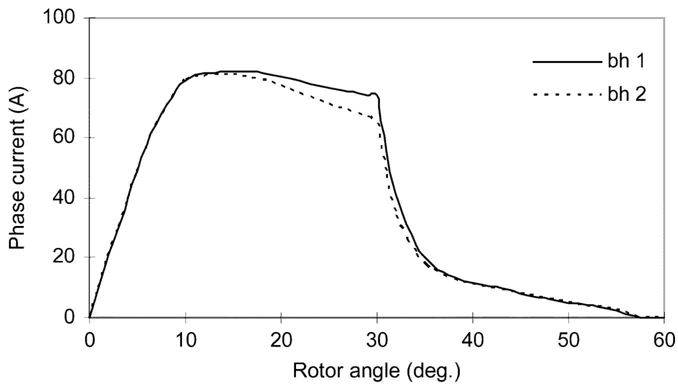

Fig. 12. Effect of different BH-curves on the simulated current waveform.

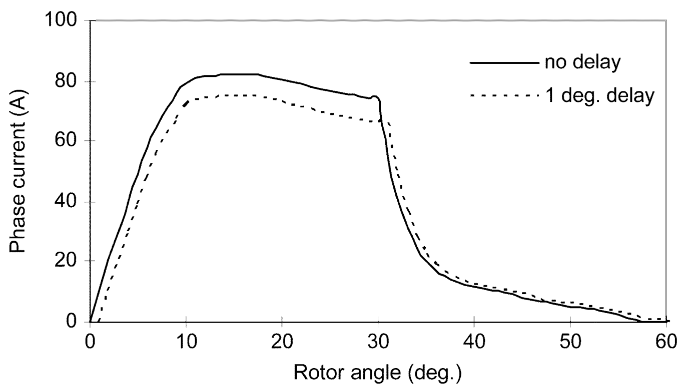

Fig. 13. Effect of switching delay of one degree on the simulated current waveform.

TABLE II
NUMBER OF SOLUTIONS AND SIMULATION TIME OF TWO METHODS

Step size (degrees)	Number of FE solutions	Average time per FE solution (s)	Simulation time (min)
Vector direction method			
1	288	4.02	19.3
3	151	4.17	10.5
5	89	4.27	6.3
Partial differential method			
1	476	3.47	27.5
3	160	3.84	10.25
5	94	3.99	6.25

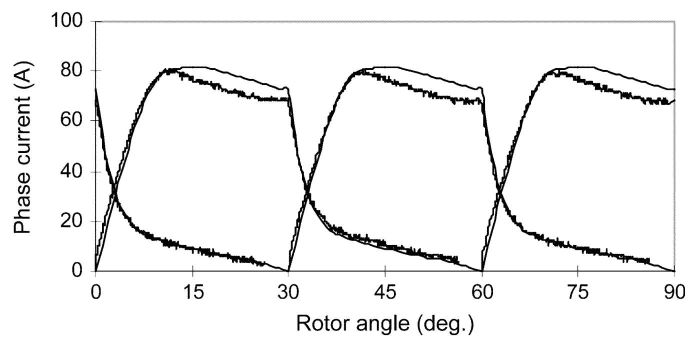

Fig. 14. Simulated and measured current waveforms of the SRM under SPMO.

the stator/rotor magnetic circuit. This will give rise to the flux linkage variation with position, $\partial\lambda/\partial\theta$, meaning a higher back EMF induced voltage that will oppose [according to (17)] the phase current, as observed in Fig. 12. Correct BH-data, hence, must be used in FE time-step current waveform simulations.

C. *Effect of Switching Delay*

The effect of a delay of only one degree in the SPMO-switching of a phase winding on the simulated current waveform is shown in Fig. 13. It is observed that such a small delay has a drastic effect on the current waveform and hence the torque of the machine. By delaying switching-on the amount of overlapping between stator and rotor poles is increased resulting in a higher phase inductance and higher back emf induced voltage. This may explain the phase current reduction effect as observed in Fig. 13. The result emphasizes that measurement of the phase current versus rotor position must be carried out accurately; otherwise significant differences between measured and calculated results will occur.

V. SIMULATION TIME

In Table II a summary is given of the number of solutions and simulation time of the two proposed methods to complete a 60° switching cycle under SPMO. A high-dense mesh was used in both methods. The simulation was done on a 3 GHz Pentium IV computer. It can be seen that the vector direction method is fast compared to the partial differential method when small step sizes are used, but equal in time when larger step sizes are used. The latter was expected as the vector direction method with larger step sizes uses more iterations to find the correct current vector.

The total simulation time is still relatively long, mainly due to the high-dense mesh used, but is expected to reduce substantially with the next generation of fast computers.

VI. SIMULATED AND MEASURED RESULTS

Measurements were taken of the phase current waveforms of the 49 kW SRM of Fig. 2 with the system in the steady state under SPMO and constant load torque. The measurements were conducted at an average speed of 1572 r/min and a dc bus voltage of 524 V. These conditions were set in the simulation of the system. The volt drop across the semi-conductor switches is accounted for in the simulation and the moment of inertia was taken as 0.8 kg·m^2. The speed variation was also simulated.

In the test, a three-phase IGBT converter with two transistors per phase (shown in Fig. 1) is used to power the SRM. A fix-point DSP controller (TMS320F240) is employed to control the switching of the transistors in SPMO via fiber optic cables. The rotor position feedback to DSP controller is generated by a resolver. For the load of the SRM drive, an eddy current dynamometer is used. The three phase currents were measured with a Tektronix TDS 460A digital oscilloscope.

The measured and simulated results of the current waveforms are shown in Fig. 14. The multiphase operation of the SRM is clear from this figure. The comparison between measured and simulated results is reasonably good if one considers e.g., the effect the BH-curve has on the simulated current waveform (see Fig. 12), and secondly the fact that 3-D and eddy current effects were ignored.

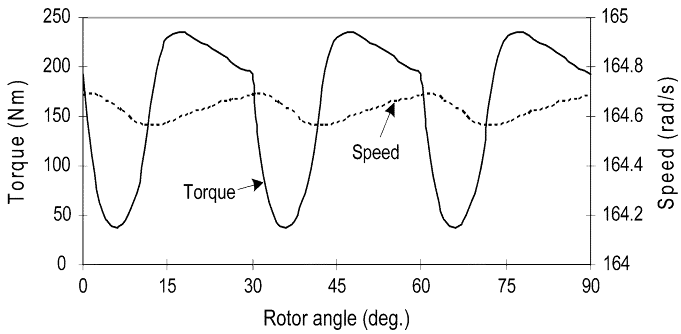

Fig. 15. Simulated torque and speed of the SRM drive under SPMO.

In Fig. 15, the torque waveform and speed of the SRM under SPMO are shown. It is clear that the ripple torque is quite high under these conditions. The simulated speed variation of the drive system is shown to be very little in this case.

VII. End Winding Effects

To take end winding effects into account, 3-D FE solutions can likewise be used in the proposed simulation methods. Obviously, the simulation time then will be much longer. To approximately compensate for end-winding effects when using 2-D FE solutions, the per phase end-winding self and mutual inductances can be calculated analytically or precalculated by 3-D FE analysis, and then added to the inductance terms of the inductance matrix of (14). Similarly, the per-phase end-winding resistance can be calculated analytically and added to the main winding resistance.

VIII. Conclusion

The proposed *vector direction* and *partial differential* FE time-step current waveform simulation methods take the effects of saturation and mutual coupling between the phases into account. Although both methods make use of the incremental inductance of the machine, the solution methodologies are different. Both methods yield practically the same simulation results if small step sizes are used, but slightly different results if large step sizes are used. The vector direction method is found to be in general the faster and better method of the two proposed methods. It is shown that the mesh and BH-curve used in the FE analysis have substantial effects, among other things, on the time-step simulation results and must be considered with care. The good comparison between the measured and simulated current waveforms in multiphase single pulse mode operation of the SRM drive verifies the proposed methods. The two methods proposed in the paper can also be used for the simulation of SRM drives under other operating modes.

Acknowledgment

This work was supported by the University of Stellenbosch, South Africa.

References

[1] J. M. Stephenson and J. Corda, “Computation of torque and current in doubly salient reluctance motors from non-linear magnetization data,” *IEE Proc.*, vol. 122, no. 5, pp. 393–396, 1979.

[2] J. Corda and S. Masic, “Computations of torque pulsations of switched reluctance drive,” in *IEE Conf. Elect. Mach. Drives*, 1989, no. 310, pp. 308–311.

[3] R. Krishnan and R. A. Bedingfield, “Dynamic analysis of an SRM drive system,” in *IEEE-IAS Annu. Meeting, Conf. Rec.*, Dearborn, MI, Oct. 1991, pp. 265–271.

[4] N. J. Nagel and R. D. Lorenz, “Modeling of a saturated switched reluctance motor using an operating point analysis and the unsaturated torque equation,” *IEEE Trans. Ind. Appl.*, vol. 36, no. 3, pp. 714–722, May/Jun. 2000.

[5] B. J. Mecrow, C. Weiner, and A. C. Clothier, “The modelling of switched reluctance machines with magnetically coupled windings,” in *IEEE-IAS Annu. Meeting, Conf. Rec.*, Rome, Italy, Oct. 2000.

[6] A. A. Arkadan and B. W. Kielgas, “Switched reluctance motor drive systems dynamic performance prediction and experimental verification,” *IEEE Trans. Energy Convers.*, vol. 9, no. 1, pp. 36–42, Mar. 1994.

[7] S. Williamson and A. F. Volschenk, “Time-stepping finite element analysis for a synchronous generator feeding a rectifier load,” *IEE Proc.-Electr. Power Appl.*, vol. 142, no. 1, pp. 50–56, Jan. 1995.

[8] L. Xu and E. Ruckstadter, “Direct modeling of switched reluctance machine by coupled field-circuit method,” *IEEE Trans. Energy Convers.*, vol. 10, no. 3, pp. 446–452, Sep. 1995.

[9] Y. Xu and D. A. Torrey, “Study of the mutually coupled switched reluctance machine using the finite element-circuit coupled method,” *IEE Proc.-Electr. Power Appl.*, vol. 149, no. 2, pp. 81–86, Mar. 2002.

[10] W. Wu, B. A. Kalan, and H. C. Lovatt, “Time-stepping analysis of a switched reluctance motor by coupling electrical circuit and electromagnetic finite element methods,” in *6th Int. Conf. Elect. Mach. Syst. (ICEMS)*, Nov. 2003, vol. 2, pp. 728–731.

[11] X. Dexin, Y. Xiuke, and Z. Yihuang, “A direct field-circuit-motion coupled modeling of switched reluctance motor,” *IEEE Trans. Magn.*, vol. 40, no. 2, pp. 573–576, Mar. 2004.

[12] J.-H. Choi, T. H. Kim, Y.-S. Kim, S.-B. Lim, S.-J. Lee, Y.-H. Kim, and J. Lee, “The finite element analysis of switched reluctance motor considering asymmetric bridge converter and dc link voltage ripple,” *IEEE Trans. Magn.*, vol. 41, no. 5, pp. 1640–1643, May 2005.

[13] J.-H. Choi, J. S. Ahn, and J. Lee, “The characteristic analysis of switched reluctance motor considering dc-link voltage ripple on hard and soft chopping modes,” *IEEE Trans. Magn.*, vol. 41, no. 10, pp. 4096–4098, Oct. 2005.

[14] A. A. Abdel-Razek, J. L. Coulomb, M. Feliachi, and J. C. Sabonnadiere, “Conception of an air-gap element for the dynamic analysis of the electromagnetic field in electric machines,” *IEEE Trans. Magn.*, vol. MAG-18, no. 2, pp. 655–659, 1982.

[15] T. J. Flack and A. F. Volschenk, “Computational aspects of time-stepping finite-element analysis using an air-gap element,” in *Proc. Int. Conf. Electrical Machines (ICEM)*, Paris, France, 1994.

[16] L. M. M. Sitsha and M. J. Kamper, “Design aspects of straight and tapered pole switched reluctance machines,” in *IEEE Africon*, Cape Town, Oct. 1999, vol. 2, pp. 683–686.

Manuscript received December 23, 2005; revised February 6, 2007. Corresponding author: M. J. Kamper (e-mail: kamper@sun.ac.za).